

Supporting Information

Insights into the Formation and Evolution of Individual Compounds in the Particulate Phase during Aromatic Photo-oxidation

Kelly L. Pereira¹, Jacqueline F. Hamilton^{1}, Andrew R. Rickard^{1,2}, William. J. Bloss³, Mohammed S. Alam³, Marie Camredon⁴, Martyn W. Ward¹, Kevin. P. Wyche⁵, Amalia Muñoz⁶, Teresa Vera⁶,
Mónica Vázquez⁶, Esther Borrás⁶, Milagros Ródenas⁶.*

¹Wolfson Atmospheric Chemistry Laboratory, Department of Chemistry, University of York, York, UK. ²National Centre for Atmospheric Science, University of York, UK. ³School of Geography, Earth and Environmental Sciences, University of Birmingham, Birmingham, UK. ⁴LISA, UMR CNRS/INSU 7583, University of Paris-Est Créteil and Paris Diderot, Créteil, France. ⁵Air Environment Research, School Environment and Technology, University of Brighton, Brighton, UK. ⁶CEAM-UMH, EUPHORE, Valencia, Spain.

*Corresponding author; e-mail: jacqui.hamilton@york.ac.uk. Phone: +44 (0)1904 324076. Fax: +44 (0) 1904 322516.

Number of pages - 30

Number of figures - 13

Number of tables - 7

Table S1 – Compound structures, most likely mechanistic generation and the time period the structurally identified TP1 compounds were first observed in the aerosol phase during MC_[high] (Table 1).

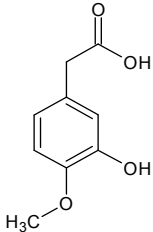
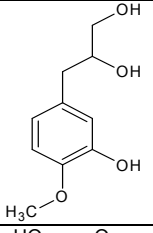
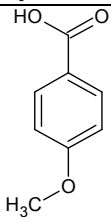
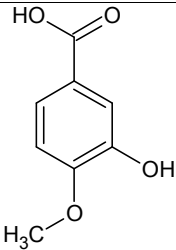
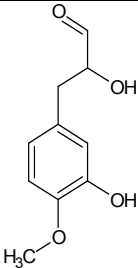
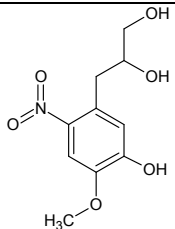
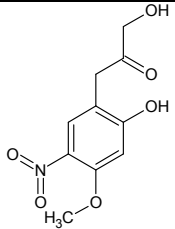
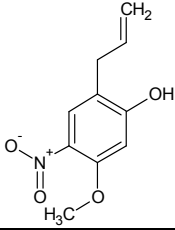
Compound nu.	IUPAC name	MW (g mol ⁻¹)	MF	Structure	First observed in the aerosol phase (minutes)	Maximum aerosol concentration (minutes)	Proposed mechanistic generation
1	(3-hydroxy-4-methoxyphenyl)acetic acid	182	C ₉ H ₁₀ O ₄		71 - 101	162 - 192	^a
2	3-(3-hydroxy-4-methoxyphenyl)propane-1,2-diol	198	C ₁₀ H ₁₄ O ₄		71 - 101	162 - 192	3 rd
3	4-methoxybenzoic acid	152	C ₈ H ₈ O ₃		71 - 101	192 - 222	^a

Table S1 - Continued

Compound nu.	IUPAC name	MW (g mol ⁻¹)	MF	Structure	First observed in the aerosol phase (minutes)	Maximum aerosol concentration (minutes)	Proposed mechanistic generation
4	3-hydroxy-4-methoxybenzoic acid	168	C ₈ H ₈ O ₄		101 - 131	192 - 222	^a
5	2-hydroxy-3-(3-hydroxy-4-methoxyphenyl)propanal	196	C ₁₀ H ₁₂ O ₄		71 - 101	222 - 252	3 rd

^a = Suspected > 4th generation species, most likely formed through the reaction with ozone¹. MW = molecular weight. MF = molecular formula.

Table S2 - Compound structures, most likely mechanistic generation and the time period the structurally identified TP3 compounds were first observed in the aerosol phase during MC_[high] (Table 1).

Compound nu.	IUPAC name	MW (g mol ⁻¹)	MF	Structure	First observed in the aerosol phase (minutes)	Maximum aerosol concentration (minutes)	Proposed mechanistic generation
1	3-(5-hydroxy-4-methoxy-2-nitrophenyl)propane-1,2-diol	243	C ₁₀ H ₁₃ NO ₆		41 - 71	71 - 101	3 rd
2	1-hydroxy-3-(2-hydroxy-4-methoxy-5-nitrophenyl)propan-2-one	241	C ₁₀ H ₁₁ NO ₆		41 - 71	71 - 101	3 rd
3	5-methoxy-4-nitro-2-(prop-2-en-1-yl)phenol	209	C ₁₀ H ₁₁ NO ₄		41 - 71	71 - 101	2 nd

MW = molecular weight. MF = molecular formula.

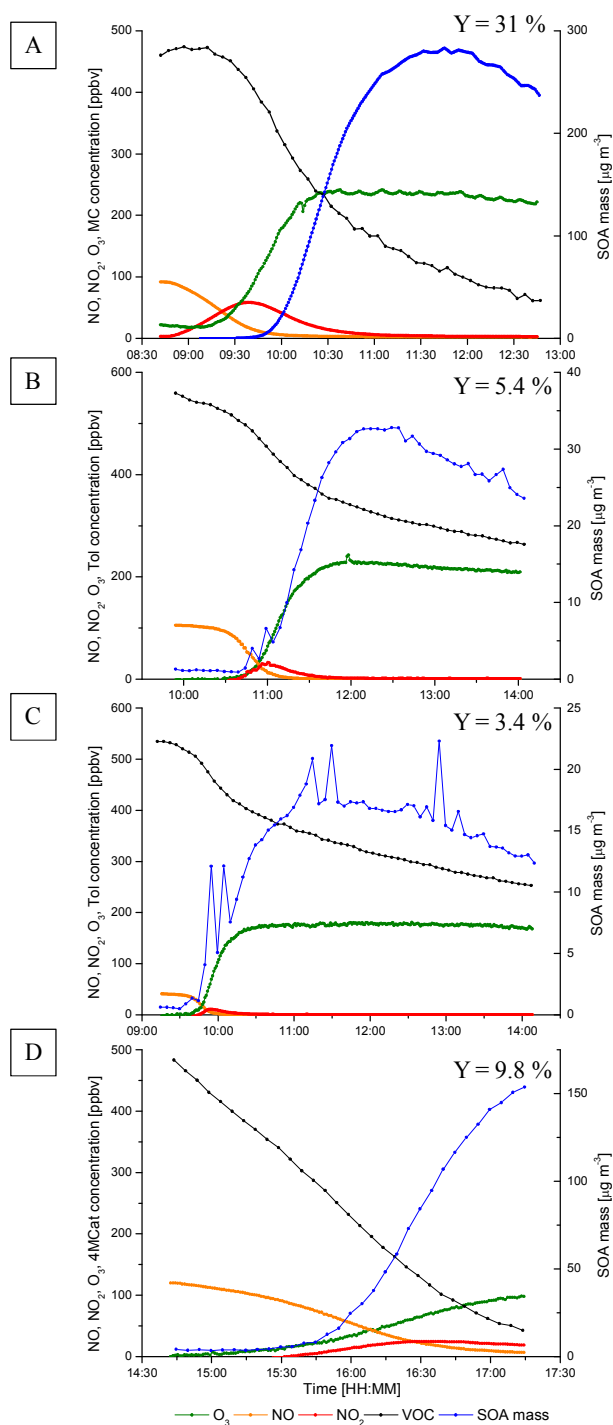


Figure S1 - Temporal profiles of the VOC precursor, NO, NO₂, O₃ and the SOA mass formed, from the opening to the closing of the chamber covers during experiment MC_{high} (A), Tol_{mod} (B), Tol_{low} (C) and 4MCat (D) (Table 1). Tol = toluene. MC = methyl chavicol. Y = SOA yield, corrected for chamber wall loss and dilution.

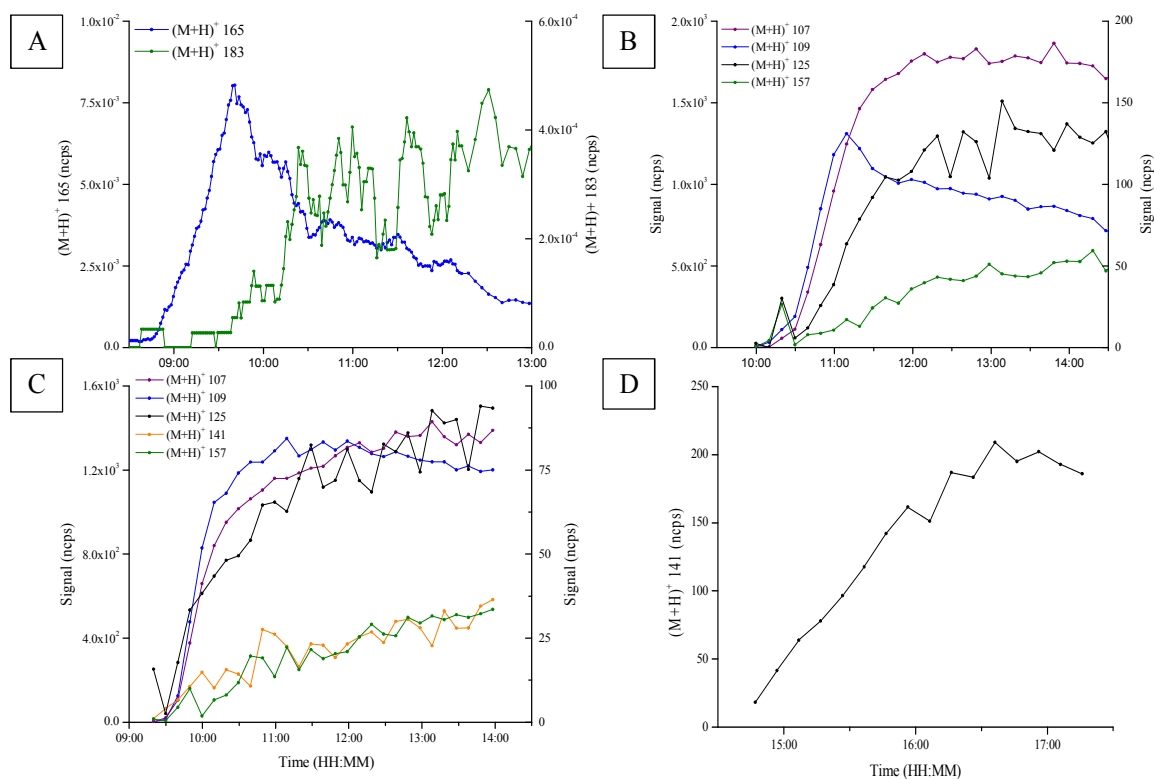


Figure S2 - First generation gas-phase photo-oxidation products observed in experiments MC_{high} (A), Tol_{mod} (B), Tol_{low} (C) and 4MCat (D) using PTR-MS or CIR-TOF-MS. Relative signal concentrations (normalised counts per second, ncps) may be attributed to; (A) (M+H)⁺ 165 = 2-methoxy-5-(prop-2-en-1-yl)phenol[†] and (M+H)⁺ 183 = 3-(4-methoxyphenyl)propane-1,2-diol. (B) and (C) (M+H)⁺ 107 = benzaldehyde, (M+H)⁺ 109 = cresol[†], (M+H)⁺ 125 = benzyl hydroperoxide, (M+H)⁺ 141 = TLEPOXMUC* and (M+H)⁺ 157 = TLBIPER2OH* (* see <http://mcm.leeds.ac.uk/MCM>). (D) (M+H)⁺ 141 = 5-methylbenzene-1,2,4-triol[†] and/or 2-hydroperoxy-4-methylphenol[†]. [†] = isomeric species. The signals of (M+H)⁺ 183 (A), (M+H)⁺ 125, (M+H)⁺ 141 and (M+H)⁺ 157 (B and C) are displayed on the secondary y-axis.

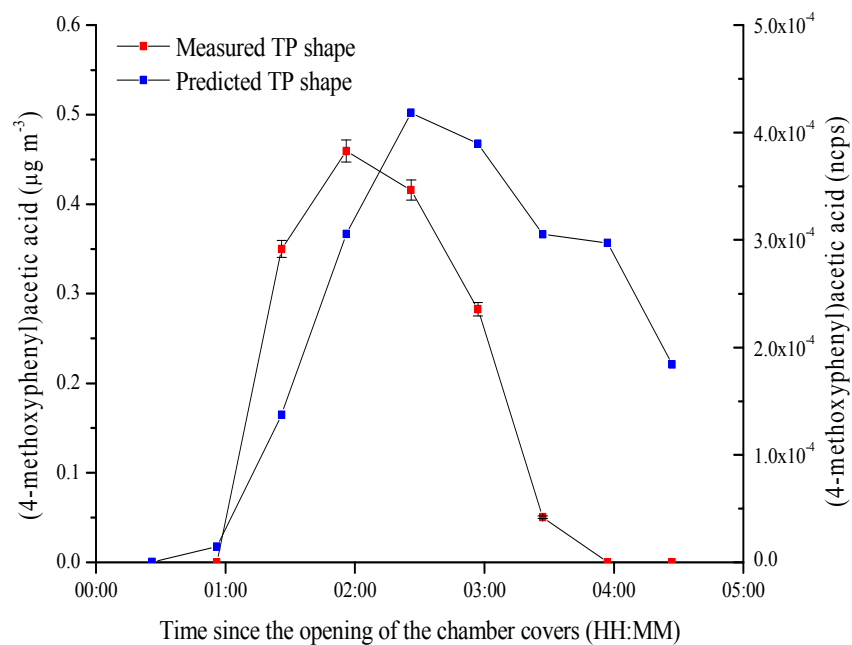


Figure S3 - Measured (primary y-axis) and predicted (secondary y-axis) particulate phase concentration of (4-methoxyphenyl)acetic acid during experiment MC_[high] (Table 1). The predicted particle phase concentration of (4-methoxyphenyl)acetic acid has been calculated using absorptive partitioning theory² and is based on the average SOA mass formed and the average relative concentration (normalised counts-per-second, ncps) of (M+H)⁺ 167 measured by the PTR-MS during each PILS sampling time period. (M+H)⁺ 167 has previously been attributed to (4-methoxyphenyl)acetic acid¹ and is the further oxidation product of 4-methoxybenzene acetaldehyde ((M+H)⁺ 151); a major methyl chavicol photo-oxidation product previously identified with PTR-MS³⁻

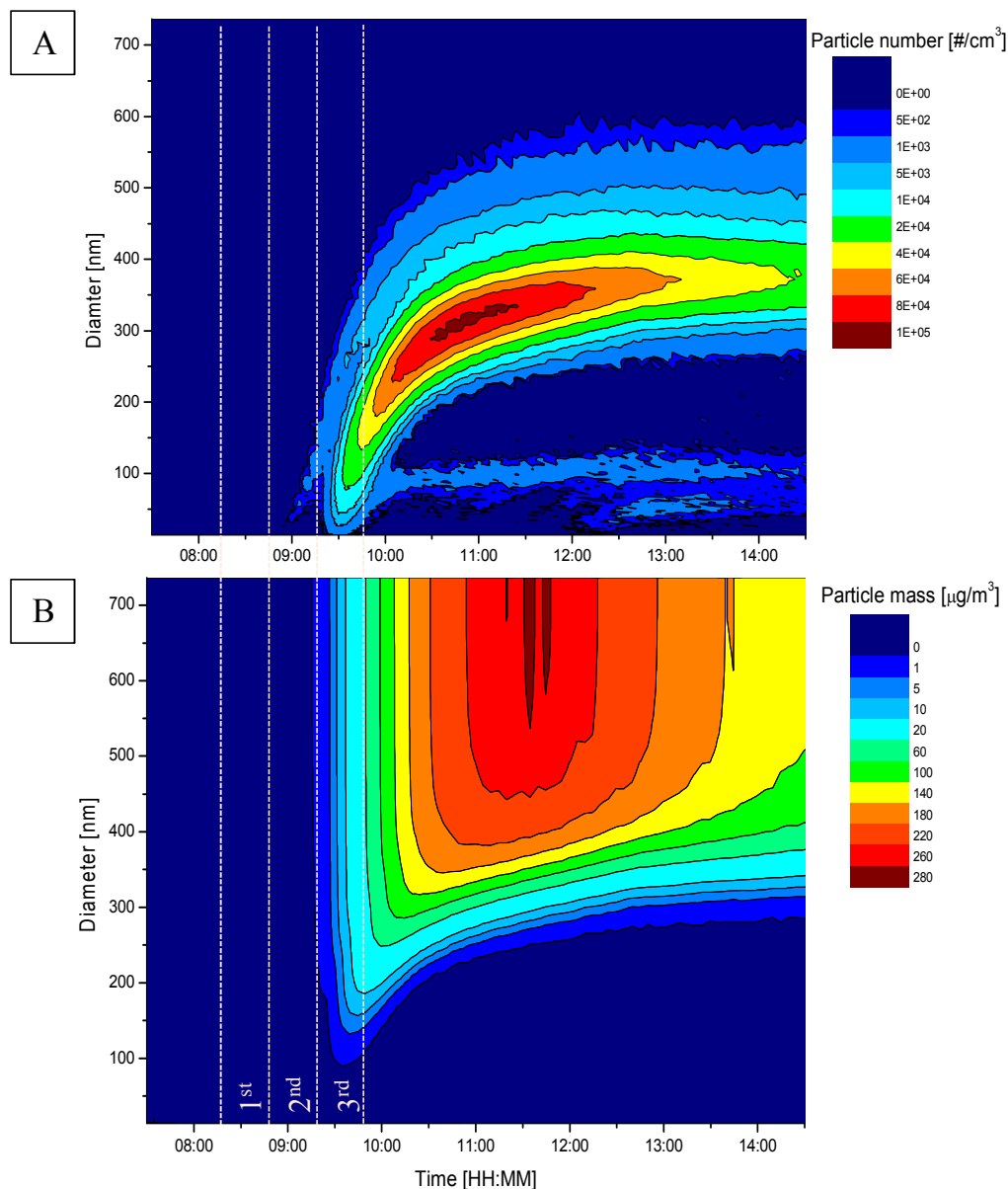


Figure S4 - Particle diameter vs. time with a coloured contour plot displaying increasing particle number (A) and particle mass (B) during $MC_{[high]}$. Dashed lines display the sampling period of the first three PILS samples from the opening of the chamber covers. Chamber covers opened at 08:42 am, 19 minutes into the first PILS sample. SOA compounds were first observed in the third PILS sample, between 41 to 71 minutes into the experiment.

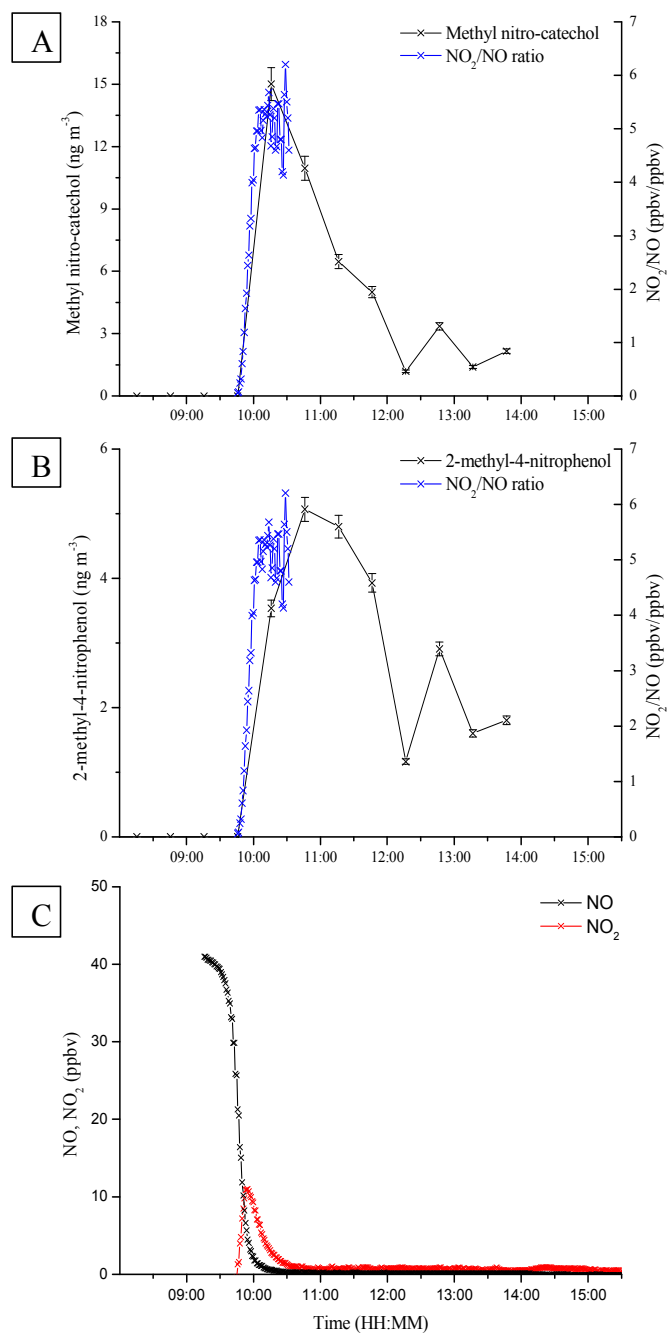


Figure S5 - Correlation of the NO₂/NO concentration ratio (ppbv/ppbv) with the particle phase temporal profiles of two toluene oxidation products, methyl nitro-catechol (suspected structure = 3-methyl-4-nitrocatechol) (A) and 2-methyl-4-nitrophenol (B) during Tol_{low}, with the NO and NO₂ temporal evolution shown in (C).

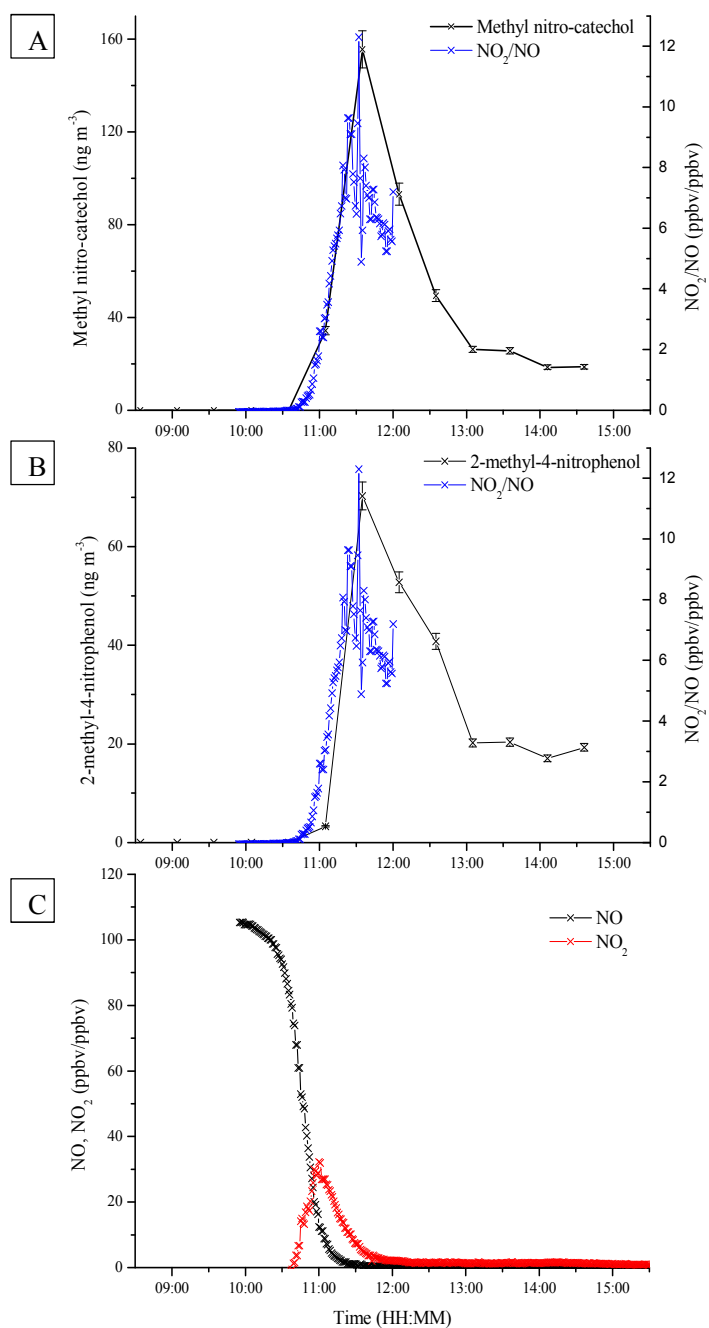


Figure S6 - Correlation of the NO₂/NO concentration ratio (ppbv/ppbv) with the particle phase temporal profiles of two toluene oxidation products, methyl nitro-catechol (suspected structure = 3-methyl-4-nitrocatechol) (A) and 2-methyl-4-nitrophenol (B) during Tol_{mod}, with the NO and NO₂ temporal evolution shown in (C).

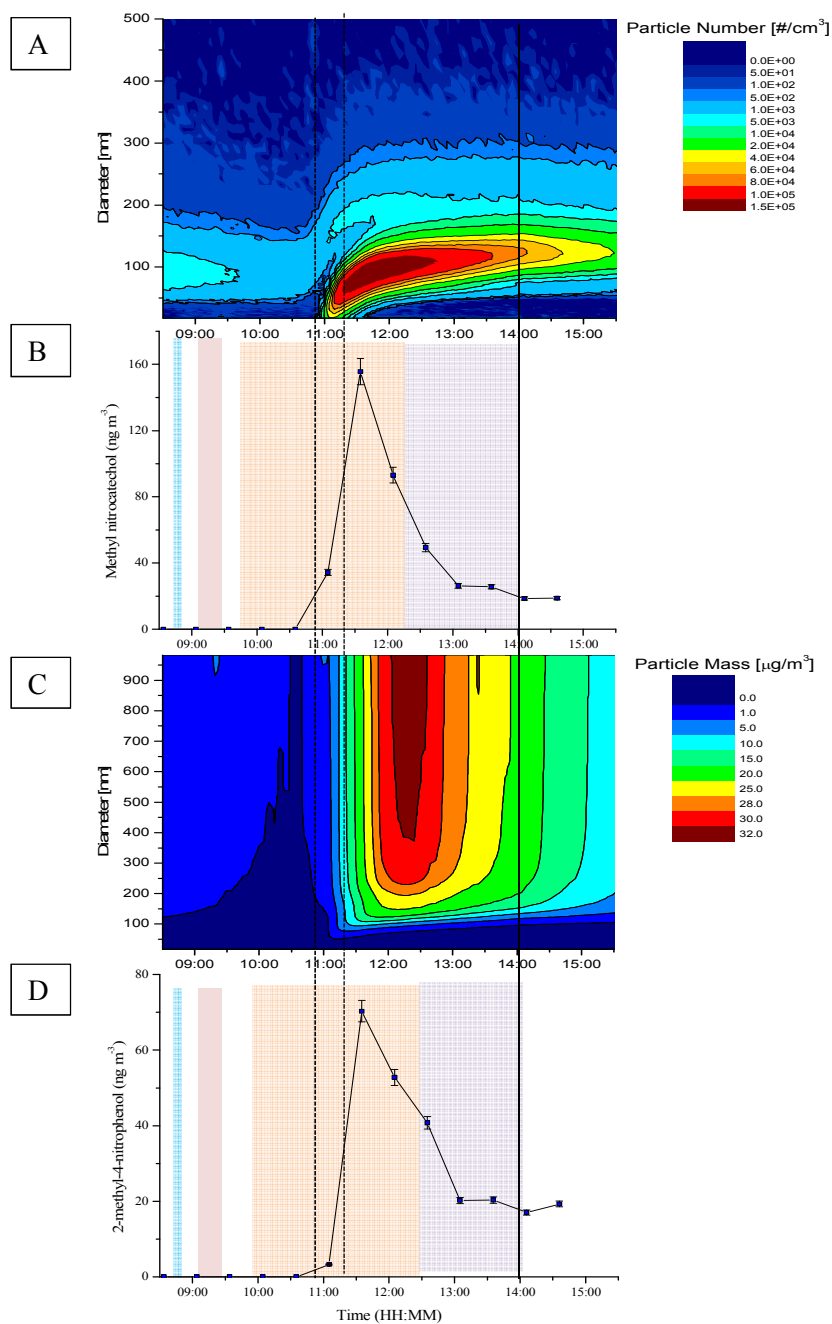


Figure S7 - Particle diameter vs. time with a coloured contour plot displaying increasing particle number (A) and particle mass (C), compared with the temporal profile of methyl nitro-catechol (suspected structure = 3-methyl-4-nitrocatechol) (B) and 2-methyl-4-nitrophenol (D) during Tol_{mod}. Shaded areas in (B) and (D); Blue = toluene addition. Red = NO addition. Orange = Chamber covers fully open. Purple = chamber cover closed by 30°. Black line = chamber covers closed. Dashed lines display the sampling period where SOA was first observed in the PILS samples.

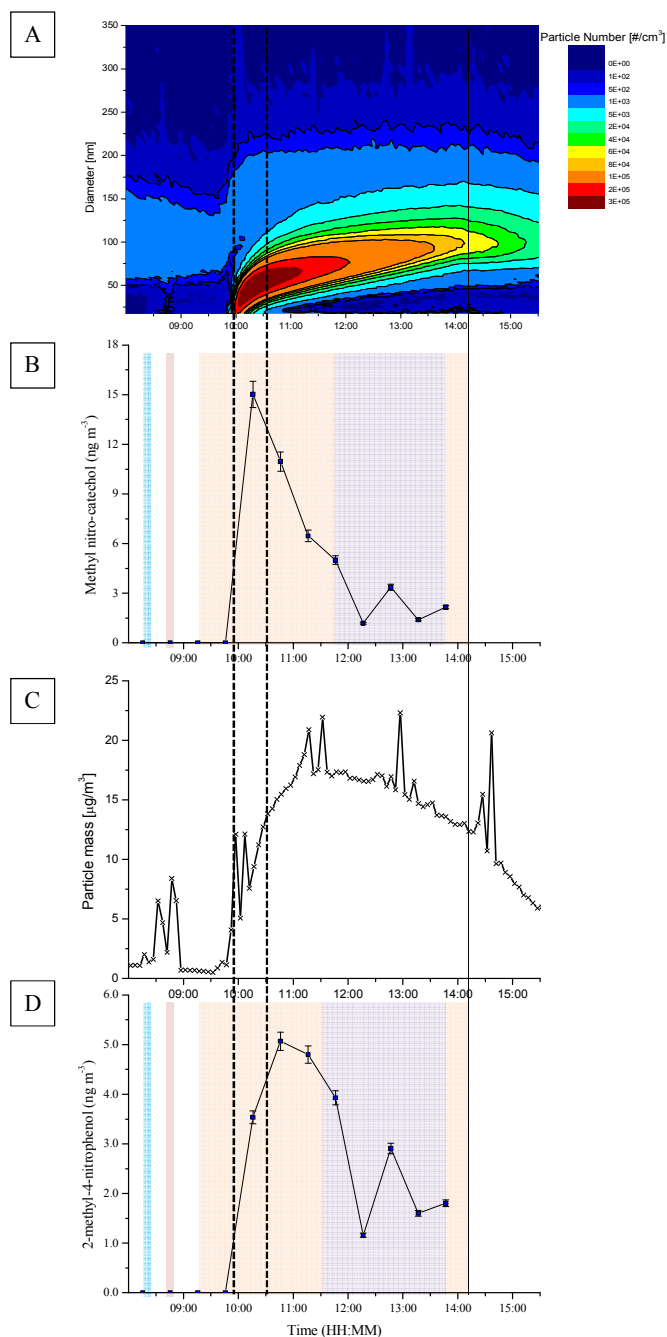


Figure S8 - Particle diameter vs. time with a coloured contour plot displaying increasing particle number (A) compared with increasing particle mass over time (C) and the temporal profile of methyl nitro-catechol (suspected structure 3-methyl-4-nitrocatechol) (B) and 2-methyl-4-nitrophenol (D) during Tol_{low}. Shaded areas in (B) and (D); Blue = toluene addition. Red = NO addition. Orange = chamber covers fully open. Purple = chamber cover closed by 30°. Black line = chamber covers closed. Dashed lines display the sampling period where SOA was first observed in the PILS samples.

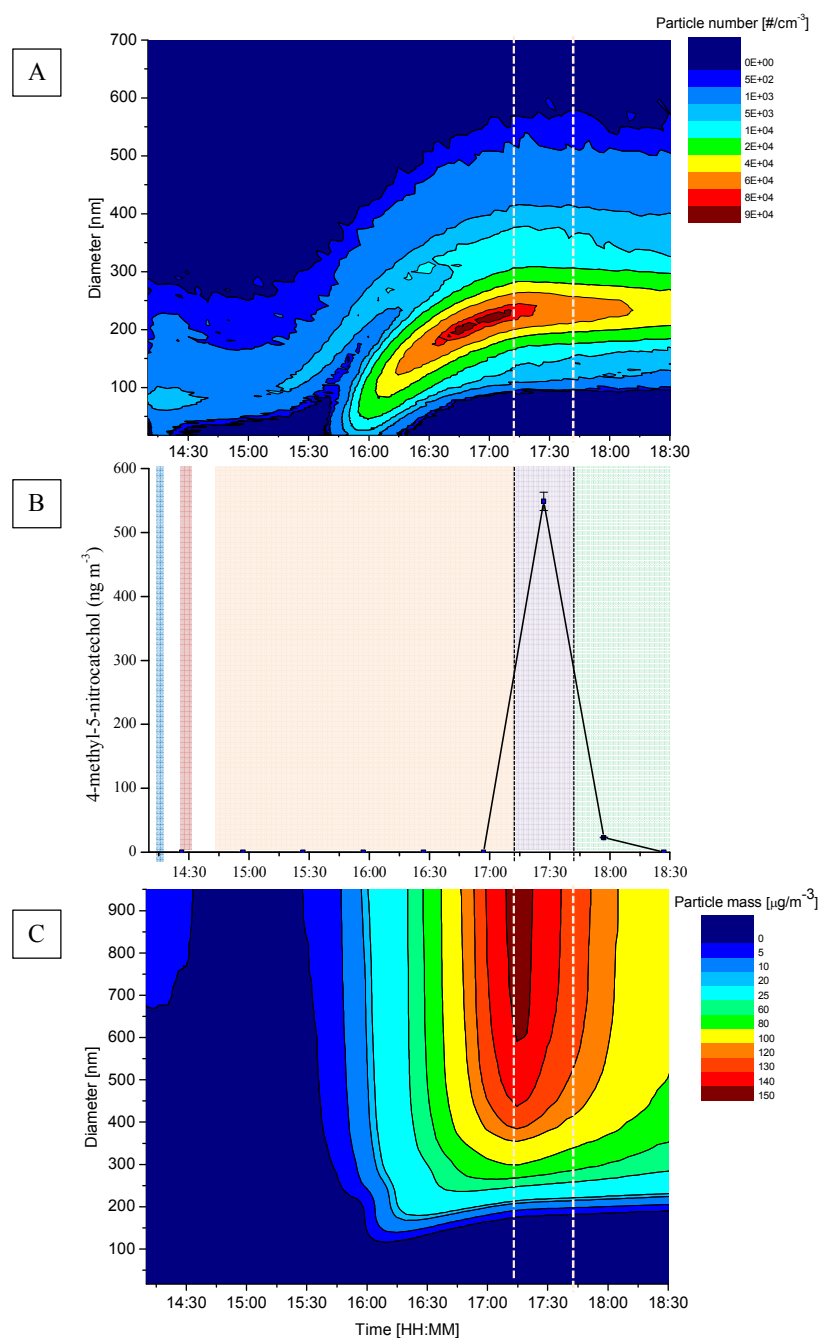


Figure S9 - Particle diameter vs. time with a coloured contour plot displaying increasing particle number (A) and particle mass (C), compared with the temporal profile of methyl nitro-catechol (suspected structure = 4-methyl-5-nitrocatechol) (B) during 4-MCat. Shaded areas in (B); Blue = 4-methyl catechol addition. Red = NO addition. Orange = chamber covers fully open. Purple = chamber cover closed. Green = filter sampling period, chamber covers still closed. Dashed lines display the start and end time of the PILS sampling period.

Photo-oxidation of methyl chavicol: Structural assignment of the nitrophenols

The fragmentation data of the structurally unidentified nitrogen containing compounds, $C_{10}H_{11}NO_4$ (MW 209 g mol⁻¹) and $C_{10}H_{11}NO_6$ (MW 241 g mol⁻¹) observed in MC_[high], are shown in Tables S3 and S4, respectively. The molecular formulae of both of these compounds were determined from the FTICR-MS and HPLC-QTOF-MS. The molecular formula of MW 209 g mol⁻¹ was determined as $C_{10}H_{11}NO_4$, with a molecular formulae error of 0.9 ppm with a score of 100 % for the FTICR-MS analysis, and an error of 6.9 ppm with a score of 100 % for the HPLC-QTOFMS analysis. The molecular formulae of MW 241 g mol⁻¹ was determined as $C_{10}H_{11}NO_6$ with an error of 0.7 ppm with a score of 100 % for the FTICR-MS analysis, and an error of -3.8 ppm with a score of 100 % for the HPLC-QTOF-MS analysis. Tentative structures have been proposed for these compounds based on the observed fragment ions and losses. The identification of both of these compounds in the first PILS SOA sample where SOA compounds were observed (*i.e.* between 41 to 71 minutes into MC_[high]) and the similarity of the carbon number and degree of saturation (DBE) to the original VOC precursor, methyl chavicol, suggests the structures of these compounds are likely to be similar to that of the VOC precursor, *i.e.* a substituted methoxyphenyl.

The proposed fragmentation of $C_{10}H_{11}NO_4$ (MW 209 g mol⁻¹) is discussed here and shown in Figure S10. This compound was assigned as 5-methoxy-4-nitro-2-(prop-2-en-1-yl)phenol (Table S2, compound 3) containing 6 DBE. The highest intensity fragment ion at m/z 193 results from an odd electron (OE) cleavage of $^{\bullet}CH_3$ from the methoxy group (R-OCH₃). OE cleavages are unusual in CID and are often associated with resonance stabilised ring structures^{1, 6}. The loss of $^{\bullet}CH_3$ suggests that a methoxy group is attached to an aromatic ring and the ring is resonance stabilised (Figure S10A). The fragment ion at m/z 178 suggests a loss of C₂H₆ from the deprotonated molecular species. This appears to be an unlikely neutral loss, suggesting that the double bond on the hydrocarbon chain (HC) has opened and gained two hydrogen atoms. Considering the gas-phase formation mechanisms, isomerisation through a 1,5 H-atom shift is suggested to be of minor importance due to the resonance stability of the ring¹. It is possible that the double bond could become saturated from the addition of

an $\cdot\text{OH}$ radical and subsequent further reactions. However, there is no indication that the hydrocarbon chain contains any elements other than carbon and hydrogen. Furthermore, the molecular formula of the remaining fragment ion, $\text{C}_8\text{H}_4\text{NO}_4$, has very few hydrogen atoms and a high number of DBE's (DBE = 7), making it difficult to propose an aromatic structure which adheres to this. A more likely alternative is the loss of NO (Figure S10B), which would also support the presence of a resonance stabilised ring structure. The loss of NO is often observed with resonance stabilised ring structures where an electron donating functional group (*e.g.* an alcohol group) is located in the para position to the nitro group^{1,6}

Fragment ion m/z 163 results from of a loss of CH_3NO from the deprotonated molecular species (Figure S10C), or a consecutive loss of NO from fragment ion m/z 193 (Figure S10D). Both losses suggest a nitro group is attached to the aromatic ring with an electron donating substituent in the para position to the nitro group. The loss of CH_3NO also supports the loss of NO from the deprotonated molecular species (fragment ion m/z 178). The loss of CH_3NO suggests the nitro group is located next to the methoxy group, undergoing an intermolecular re-arrangement and resulting in the loss of CH_3 from the methoxy group and NO from the nitro group (Figure S10C). Fragment ion m/z 145 is the result of a consecutive loss of H_2O and CH_3NO (CH_5NO_2) from the deprotonated molecular species (Figure S10D), or the loss of H_2O from fragment ion m/z 163 (Figure 10C). Hydrogen atom abstraction directly from a resonance stabilised aromatic ring is unlikely. However, if the NO_2 group has already been lost, the decrease in resonance stabilisation is more likely to allow H-atom abstraction to occur directly from the ring. Alternatively, H-atom abstraction may occur from the HC chain, resulting in the loss of H_2O .

The proposed fragmentation of $\text{C}_{10}\text{H}_{11}\text{NO}_6$ (MW 241 g mol^{-1}) is shown in Figure S11. The deprotonated molecular species $(\text{M}-\text{H})^-$ at m/z 240 was observed below the MS^2 threshold in the HPLC-QTOFMS² analysis. Consequently, the fragmentation data could not be obtained for this compound using this technique. Instead, the HPLC-ITMS² was used. This compound was assigned as 1-hydroxy-3-(2-hydroxy-4-methoxy-5-nitrophenyl)propan-2-one (Table S2, compound 2) containing

6 DBE. The highest intensity fragment ion at m/z 222 is from the loss of H_2O , suggesting the presence of an alcohol group on the hydrocarbon chain, most likely in the terminal position¹ (Figure S11A). The second fragment ion at m/z 210, suggests the loss of NO , which is further supported by the loss of CH_3NO , resulting in a fragment ion at m/z 195 (Figures S11B and C). This suggests that an NO_2 group is located on the aromatic ring next to the methoxy group and an electron donating substituent is in the para position to the NO_2 group; as observed with the fragmentation of 5-methoxy-4-nitro-2-(prop-2-en-1-yl)phenol discussed above.

The fragment ion at m/z 193 can be attributed to the loss of HNO_2 , which most likely results from the NO_2 group abstracting a hydrogen atom from the methoxy group (Figure S11D). Finally, the fragment ion at m/z 166 can be attributed to the loss of $C_3H_6O_2$ from the deprotonated molecular species, which is mostly likely to be the loss of the hydrocarbon chain. The loss of $C_3H_6O_2$ contains too few hydrogen atoms to be fully saturated. Furthermore, the loss of H_2O (fragment ion m/z 222), suggests that the double bond on the hydrocarbon chain has opened. Therefore, it is likely that a ketone is attached on the adjacent carbon atom to the alcohol group (Figure S11E), with the leaving group ($C_3H_6O_2$) abstracting a hydrogen atom from the aromatic ring, most likely after the loss of NO_2 .

Table S3 - Deprotonated molecular species fragmentation for C₁₀H₁₁NO₄ (MW 209 g mol⁻¹), obtained from the use of the HPLC-ITMS² and the HPLC-QTOFMS²

[M-H] ⁻	<i>m/z</i>	DBE	Fragment ion (<i>m/z</i>)	Fragment ion MF	DBE	EF	Loss (Da)	Suspected loss	Fragment ion MF error (ppm)	Fragment ion score [%]	Fragmentation shown
C ₁₀ H ₁₀ NO ₄	208	6	193	C₉H₇NO₄	6*	OE	15	•CH₃	7.0	100	Figure S10A
			178	C ₈ H ₄ NO ₄	7	EE	30	C ₂ H ₆ †	5.7	100	Figure S10B
			163	C ₉ H ₇ O ₃	6	EE	45	CH ₃ NO or NO from <i>m/z</i> 193	-0.1	100	Figure S10C
			145	C ₉ H ₅ O ₂	7	EE	63	CH ₅ NO ₂ (H ₂ O + CH ₃ NO) or H ₂ O from <i>m/z</i> 163	2.7	100	Figure S10 C and D

The highest intensity fragment ion is shown in bold. MF = molecular formula. Electron fragmentation (EF), EE = even electron, OE = odd electron. *DBE was manually calculated, as automated DBE calculation is incorrect for radical fragment ions (DBE = 6.5 - 0.5 (for one ‘hydrogen atom deficiency’) = 6; see Pellegrin (1983)⁷ for the calculation of DBE and DBE correction for radical ions). † = Loss of C₂H₆ seems unlikely, suspected loss of NO (see text for further explanation).

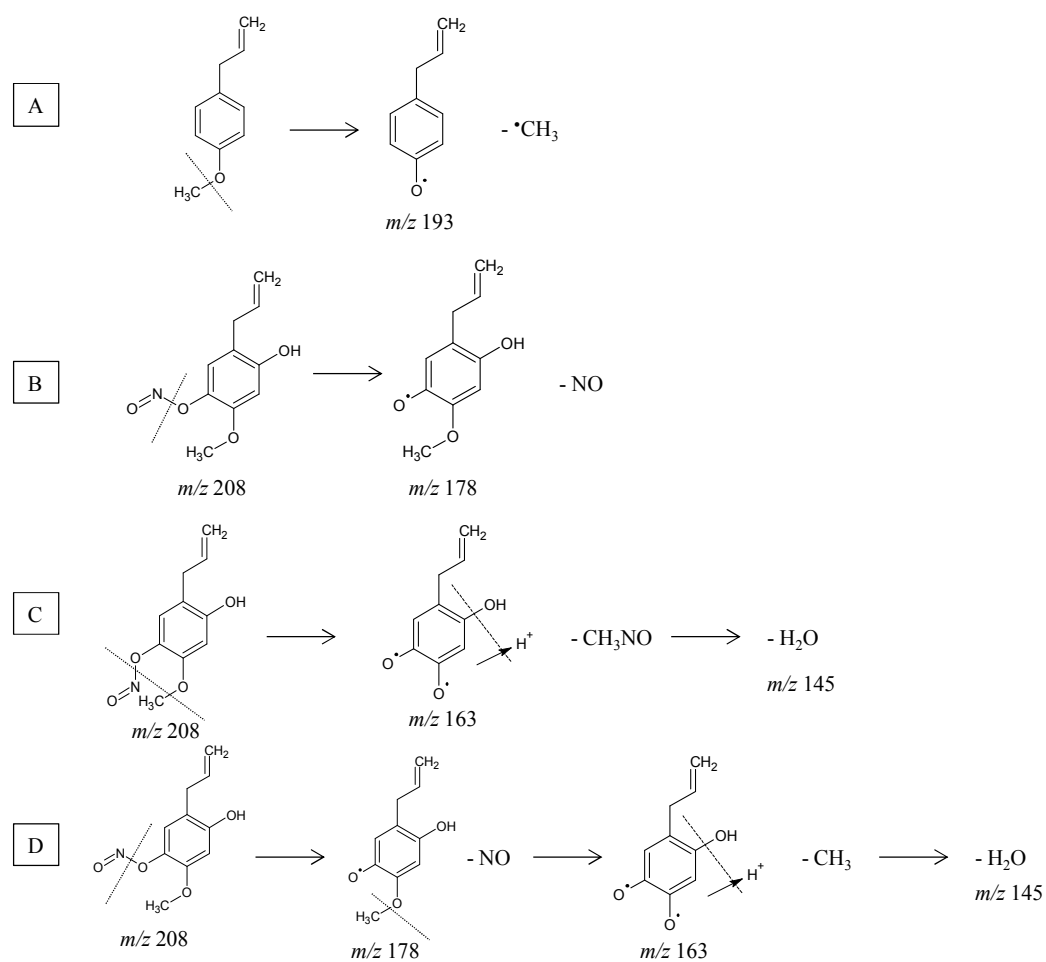


Figure S10 - Proposed deprotonated molecular species fragmentation for $\text{C}_{10}\text{H}_{11}\text{NO}_4$ (MW 209 g mol^{-1}) in negative ionisation mode. Dashed lines indicate the location of fragmentation.

Table S4 - Deprotonated molecular species fragmentation for C₁₀H₁₁NO₆ (MW 241 g mol⁻¹), obtained from the use of the HPLC-ITMS²

(M-H) ⁻	Fragment ion (<i>m/z</i>)	Loss (Da)	Suspected loss	Fragmentation shown
240	222	18	H₂O	Figure S11A
	210	30	NO	Figure S11B
	195	45	CH ₃ NO	Figure S11C
	193	47	HNO ₂	Figure S11D
	166	74	C ₃ H ₆ O ₂	Figure S11E

MW = molecular weight. The highest intensity fragment ion is shown in bold.

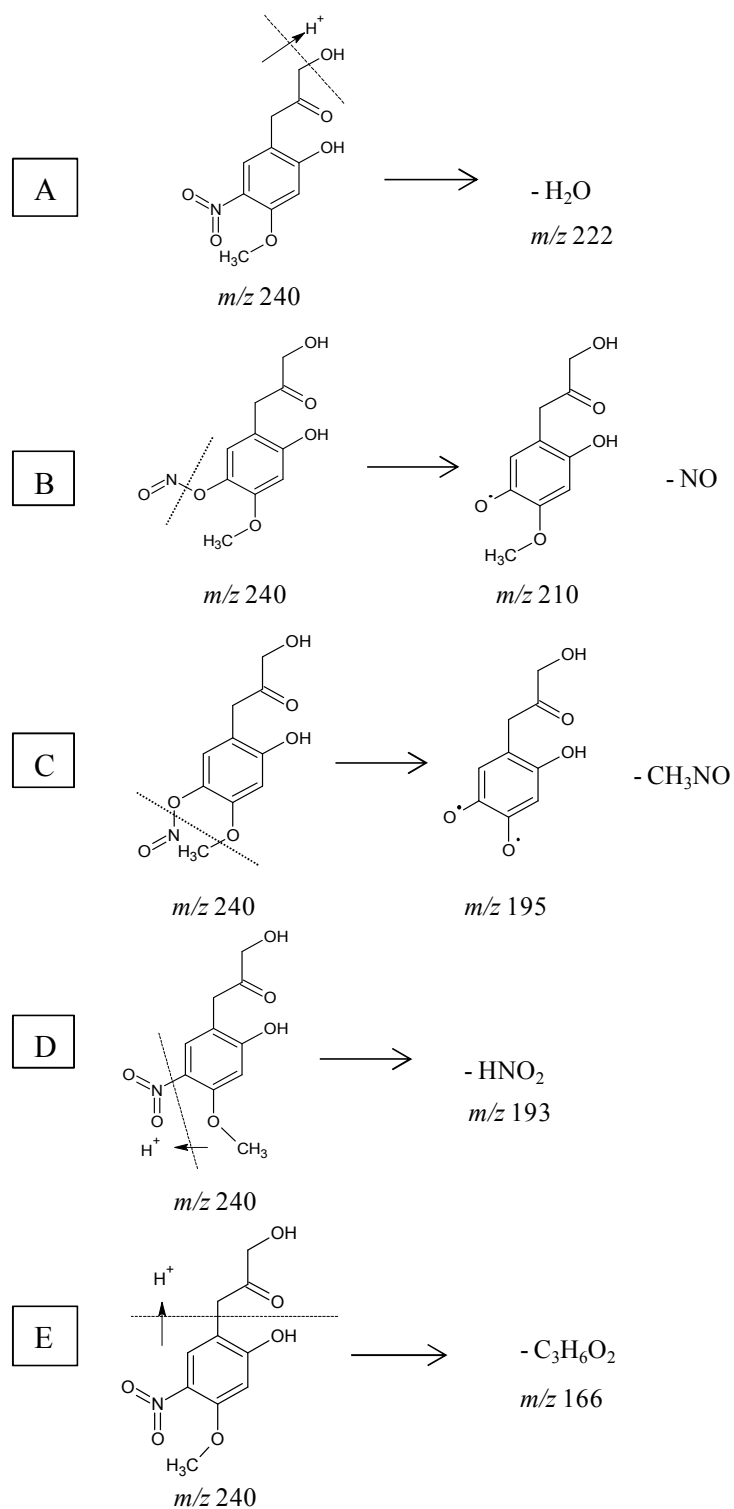


Figure S11 - Proposed deprotonated molecular species fragmentation for C₁₀H₁₁NO₆ (MW 241 g mol⁻¹) in negative ionisation mode. Dashed lines indicate the location of fragmentation.

Photo-oxidation of methyl chavicol: Fragmentation of the suspected nitrophenols

Three compounds, $C_9H_{11}NO_9$ (t_R 11.8), $C_9H_{11}NO_9$ (t_R 12.8) and $C_{10}H_9NO_3$ all displayed characteristic mass spectral fragmentation patterns suggesting that these species contained a resonance stabilised ring structure and a nitro-group. The fragment ions and respective losses observed for the three structurally unidentified organic nitrogen compounds are shown below.

1. $C_9H_{11}NO_9$ (t_R 11.8) (M-H)⁻ 276 (DBE = 5)

m/z 258 = H_2O

m/z 246 = NO - Intermolecular re-arrangement of the nitro-group, which is indicative of a resonance stabilised ring structure.

m/z 231 = CH_3NO - Nitro group most likely located next to the methoxy group.

m/z 229 = HNO_2

2. $C_9H_{11}NO_9$ (t_R 12.8) (M-H)⁻ 276 (DBE = 5)

m/z 245 = HNO

m/z 229 = HNO_2 - Contains a nitro functional group.

m/z 200 = $C_3H_8O_2$ - Loss of the hydrocarbon chain, suggesting the aromatic ring is intact.

$C_{10}H_9NO_3$ (t_R 17.6) (M-H)⁻ 190 (DBE = 7)

m/z 175 = $^{\cdot}CH_3$ - Indicative of resonance stabilised ring structure.

m/z 160 = NO - Intermolecular re-arrangement of the nitro-group, suggests an electron donating substituent is in the para position to the nitro group (*i.e.* an alcohol group)

m/z 145 = CH_3NO - Nitro group most likely located next to the methoxy group.

Photo-oxidation of toluene and 4-methyl catechol: ON compound structure assignment

The deprotonated molecular species fragmentation data obtained from the HPLC-ITMS² analysis for the toluene photo-oxidation product with a MW of 168 g mol^{-1} is shown in Table S5 and the proposed

fragmentation is shown in Figure S12. This compound was assigned as 3-methyl-4-nitrocatechol. The fragment ion at m/z 138 is due to the loss of NO. As previously discussed, the loss of NO occurs from the intermolecular re-arrangement of R-NO₂ to R-O-N=O which is resonance stabilised through an electron donating substituent (*i.e.* an alcohol group) in the para position to the NO₂ group (Figure S12B). The fragment ion at m/z 123 is due to the loss of CH₃NO from the deprotonated molecular species, suggesting the NO₂ group is located adjacent to the methyl group, as shown in Figure S12C. This is further supported by the fragment ion at m/z 121 which is due to the loss of HNO₂ (Figure S12D) and the fragment ion at m/z 107 which is due to the loss of CH₃NO₂ (Figure 11E). The fragment ion at m/z 148 can be attributed to the loss of H₂O occurring through H-atom abstraction. This loss suggests an alcohol group is attached to the aromatic ring and is most likely located next to the methyl group; where hydrogen atom abstraction would be more favoured than from the resonance the stabilised ring structure (Figure S12A). This is also supported by considering the gas-phase mechanisms of formation, where the initial addition of an OH radical to toluene would be most favoured in the ortho position to the methyl group^{8,9}. Thus, based on the fragmentation patterns and gas-phase mechanisms of formation, the most likely compound structure is 3-methyl-4-nitrocatechol.

The deprotonated molecular species fragmentation data obtained from the HPLC-ITMS² analysis for the 4-methyl catechol photo-oxidation product with a MW of 168 g mol⁻¹ is shown in Table S6 and the proposed fragmentation is shown in Figure S13. This compound was assigned as 4-methyl-5-nitrocatechol. For this compound, only the location of the NO₂ group is required. The same fragment ions at m/z 138 (Figure S13A), m/z 123 (Figure S13B) and m/z 121 (Figure S13C) as observed with 3-methyl-4-nitrocatechol (toluene photo-oxidation product) were observed for fragmentation of 4-methyl-5-nitrocatechol. This suggests that the NO₂ group is located in the ortho position to the methyl group and an electron donating substituent is in the para position to the NO₂ group. Considering this, the most likely compound structure is 4-methyl-5-nitrocatechol.

Table S5 - Deprotonated molecular species fragmentation for the toluene oxidation product with a MW of 169 g mol⁻¹, obtained from the use of the HPLC-ITMS²

(M-H) ⁻	Fragment ion (<i>m/z</i>)	Loss (Da)	Suspected loss	Fragmentation shown
168	148	20 [*]	H ₂ O	Figure S12A
	138	30	NO	Figure S12B
	123	45	CH₃ from <i>m/z</i> 138 or CH₃NO	Figure S12C
	121	47	HNO ₂	Figure S12D
	107	61	CH ₃ NO ₂	Figure S12E

The highest intensity fragment ion is shown in bold. * = attributed to the loss of H₂O.

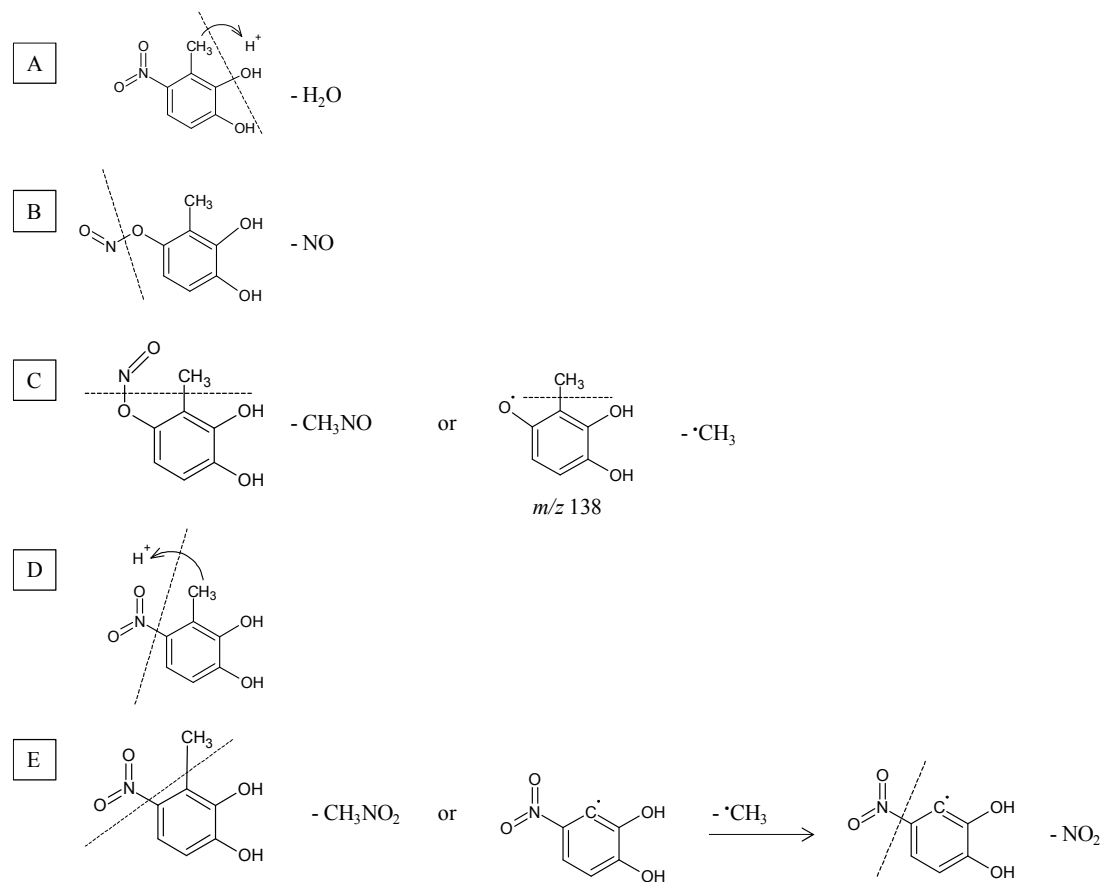


Figure S12 - Proposed deprotonated molecular species fragmentation for the toluene oxidation product with a MW of 169 g mol⁻¹ in negative ionisation mode. Dashed lines indicate the location of fragmentation.

Table S6 - Deprotonated molecular species fragmentation for the 4-methyl catechol oxidation product with a MW of 169 g mol⁻¹ obtained from the use of the HPLC-ITMS².

(M-H) ⁻	Product ion (<i>m/z</i>)	Loss (Da)	Suspected loss	Fragmentation shown
168	148	20*	H ₂ O	Figure S13A
	138	30	NO	Figure S13B
	123	45	CH ₃ from <i>m/z</i> 138 or CH ₃ NO	Figure S13C
	121	47	HNO ₂	Figure S13D

The highest intensity fragment ion is shown in bold. * = attributed to the loss of H₂O.

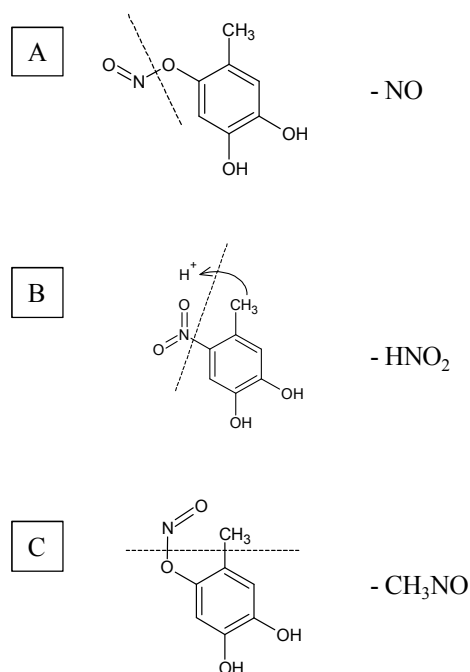


Figure S13 - Proposed deprotonated molecular species fragmentation of the 4-methyl catechol photo-oxidation product with a MW of 169 g mol⁻¹ in negative ionisation mode. Dashed lines indicate the location of fragmentation.

PILS collection efficiency and particle wall loss corrections

The PILS collection efficiency has previously been determined, where no appreciable loss has been found for the particle size range investigated (30 nm to 1 µm)¹⁰. However, it should be noted that in the PILS condensation chamber, sampled aerosol particles are mixed with a turbulent heated airflow of steam (100°C). Whilst the residence time within the condensation chamber is < 1 second¹¹, losses of volatile or thermally unstable species within the sampled aerosol particles may be observed (see Zhang et al (2015)¹¹ for further information). In addition, hydrolysis prone compounds may lead to a source of artifacts in the samples. No wall loss or chamber dilution corrections have been applied to any of the temporal profiles, aerosol mass and particle number concentrations shown in this work (with the exception of the SOA yields, where chamber wall loss and dilution corrections were applied). This procedure was followed as it was not known if the aerosol composition was consistent

across the sampled particle size range and thus, size dependant wall loss corrections could not be applied.

Volatility calculations

The vapour pressures of the structurally identified compounds were calculated using the UManSysProp online facility for calculating properties of individual organic molecules and ensemble mixtures (<http://umansysprop.seaes.manchester.ac.uk/>), employing the Nannoolal vapour pressure¹² and boiling point¹³ extrapolation method. It should be noted that the UManSysProp website which uses the structure activity relationship to calculate the vapour pressure, is based on a limited number of available experimental measurements of nitro-containing compounds.

Compound quantification

The standards used to quantify the compounds observed in MC_[high], Tol_{mod}, Tol_{low} and 4-MCat are shown in Table S7. Calibrations were performed for all of the standards shown in Table S7 and consisted of a minimum of 5 concentrations with three replicate injections for each concentration. The error bars on the temporal profiles represent the average percentage relative standard deviation from the calibration used to quantify the compound.

Table S7 - Standards used to quantify the compounds observed in MC_[high], Tol_{mod}, Tol_{low} and 4-MCat

Experiment	Compound/s quantified	Standard used
MC _[high]	Organic nitrogen compounds	2,6-dimethyl-3-nitrophenol (95 %)
	4-methoxybenzoic acid	4-methoxybenzoic acid (99 %)
	(4-methoxyphenyl)acetic acid	(4-methoxyphenyl)acetic acid (99%).
	(3-hydroxy-4-methoxyphenyl)acetic acid	(4-methoxyphenyl)acetic acid (99%).
	3-hydroxy-4-methoxybenzoic acid	4-methoxybenzoic acid (99 %)
Tol _{low} and Tol _{mod}	2-methyl-4-nitrophenol	2-methyl-4-nitrophenol (97 %)
	methyl nitro-catechol	4-nitrocatechol (95%)
4-MCat	methyl nitro-catechol	4-nitrocatechol (95%)

All compounds were purchased from Sigma Aldrich, UK. Compound purity is shown in brackets.

Supporting calculations

Predicted and measured methyl-nitrophenol aerosol phase concentration

The particle phase concentration of 2-methyl-4-nitrophenol during initial aerosol growth in experiments Tol_{low} and Tol_{mod} can be predicted by considering the amount of toluene reacted, the nitrophenol product yield and the amount of absorptive mass present. The concentration of toluene in the chamber was monitored using FTIR with a 5-minute time resolution. The amount of toluene reacted ($Tol_{reacted}$, $\mu\text{g m}^{-3}$) by the end of PILS sampling time period when SOA formation in the chamber was first observed, was calculated using Eq. 1; where $Tol_{initial}$ is the concentration of toluene upon the opening of the chamber covers ($\mu\text{g m}^{-3}$) and $Tol_{(tx)}$ is the concentration of toluene at the end of the PILS sampling time (t) period (x) ($\mu\text{g m}^{-3}$).

$$\text{Eq. 1} \quad Tol_{reacted} = Tol_{initial} - Tol_{(tx)}$$

The photo-oxidation of toluene results in the formation of methyl nitrophenol with a yield (Y) of 1.31 %, based on the information provided in the Master Chemical Mechanism (MCM) version 3.3^{14, 15} (<http://mcm.leeds.ac.uk/MCM>). The total mass concentration (gas + aerosol) ($C_{i,tot}$, $\mu\text{g m}^{-3}$) of species i (*i.e.* methyl nitrophenol) can be calculated as shown in Eq. 2.

$$\text{Eq. 2} \quad C_{i,tot} = \frac{Tol_{reacted}}{100} \times Y$$

Once $C_{i,tot}$ is known, the fraction of species i in the aerosol phase (F_i) can be calculated using Eq. 3; where C_i^* is the calculated saturation concentration of species i ($\mu\text{g m}^{-3}$) and C_{OA} is the amount of SOA mass formed by the end of the PILS sampling time period (tx) ($\mu\text{g m}^{-3}$). Multiplying F_i by $C_{i,tot}$ gives the predicted concentration of species i in the aerosol phase ($C_{i,aer(predicted)}$, $\mu\text{g m}^{-3}$), as shown in Eq. 4.

$$\text{Eq. 3} \quad F_i = \frac{1}{1 + C_i^*/C_{OA(tx)}}$$

$$\text{Eq. 4} \quad C_{i,aer(predicted)} = F_i \times C_{i,tot}$$

The predicted aerosol phase concentration of 2-methyl-4-nitrophenol during initial aerosol growth in experiments Tol_{low} and Tol_{mod} was 0.49 ng m⁻³ and 0.33 ng m⁻³, respectively. The measured aerosol phase concentration of 2-methyl-4-nitrophenol during the same time period was 8.6 times greater than the predicted concentration in Tol_{low} (measured $C_{i,aer} = 3.53 \text{ ng m}^{-3}$) and 13.9 times greater in Tol_{mod} (measured $C_{i,aer} = 3.27 \text{ ng m}^{-3}$). The large discrepancy in the predicted and measured aerosol phase concentrations of 2-methyl-4-nitrophenol suggests that this compound does not adhere to gas-particle absorption, partitioning more of its mass into the aerosol phase than can be explained by the amount of SOA mass present during this time period. These calculations were not performed for the third generation product, methyl nitro-catechol, due to the lack of toluene product yields available for this species, as a result of insufficient gas-phase measurements.

References

1. Pereira, K. L.; Hamilton, J. F.; Rickard, A. R.; Bloss, W. J.; Alam, M. S.; Camredon, M.; Muñoz, A.; Vázquez, M.; Borrás, E.; Ródenas, M., Secondary organic aerosol formation and composition from the photo-oxidation of methyl chavicol (estragole). *Atmos. Chem. Phys.* **2014**, *14*, (11), 5349.
2. Stanier, C. O.; Donahue, N.; Pandis, S. N., Parameterization of secondary organic aerosol mass fractions from smog chamber data. *Atmos. Environ.* **2008**, *42*, (10), 2276.
3. Lee, A.; Goldstein, A. H.; Kroll, J. H.; Ng, N. L.; Varutbangkul, V.; Flagan, R. C.; Seinfeld, J. H., Gas-phase products and secondary aerosol yields from the photooxidation of 16 different terpenes. *J. Geophys. Res.* **2006**, *111*, (D17), D17305.
4. Holzinger, R.; Lee, A.; Paw, K.; Goldstein, U., Observations of oxidation products above a forest imply biogenic emissions of very reactive compounds. *Atmos. Chem. Phys.* **2005**, *5*, (1), 67.

5. Bouvier-Brown, N.; Goldstein, A.; Worton, D.; Matross, D.; Gilman, J.; Kuster, W.; Welsh-Bon, D.; Warneke, C.; de Gouw, J.; Cahill, M., Methyl chavicol: Characterization of its biogenic emission rate, abundance, and oxidation products in the atmosphere. *Atmos. Chem. Phys.* **2009**, *9*, 2061.
6. Bursey, M. M., Influence of steric inhibition of resonance on ion intensities in mass spectra. *J. Am. Chem. Soc.* **1969**, *91*, (7), 1861.
7. Pellegrin, V., Molecular formulas of organic-compounds - the nitrogen rule and degree of unsaturation. *J. Chem. Educ.* **1983**, *60*, (8), 626.
8. Nakao, S.; Clark, C.; Tang, P.; Sato, K.; Cocker Iii, D., Secondary organic aerosol formation from phenolic compounds in the absence of nox. *Atmos. Chem. Phys.* **2011**, *11*, (20), 10649.
9. Forstner, H. J.; Flagan, R. C.; Seinfeld, J. H., Secondary organic aerosol from the photooxidation of aromatic hydrocarbons: Molecular composition. *Environ. Sci. Technol.* **1997**, *31*, (5), 1345.
10. Orsini, D. A.; Ma, Y.; Sullivan, A.; Sierau, B.; Baumann, K.; Weber, R. J., Refinements to the particle-into-liquid sampler (pils) for ground and airborne measurements of water soluble aerosol composition. *Atmos. Environ.* **2003**, *37*, (9), 1243.
11. Zhang, X.; Dalleska, N. F.; Huang, D. D.; Bates, K. H.; Sorooshian, A.; Flagan, R. C.; Seinfeld, J. H., Time-resolved molecular characterization of organic aerosols by pils + uplc/esi-q-tofms. *Atmos. Environ.*
12. Nannoolal, Y.; Rarey, J.; Ramjugernath, D., Estimation of pure component properties: Part 3. Estimation of the vapor pressure of non-electrolyte organic compounds via group contributions and group interactions. *Fluid Phase Equilib.* **2008**, *269*, (1), 117.

13. Nannoolal, Y.; Rarey, J.; Ramjugernath, D.; Cordes, W., Estimation of pure component properties: Part 1. Estimation of the normal boiling point of non-electrolyte organic compounds via group contributions and group interactions. *Fluid Phase Equilib.* **2004**, 226, (0), 45.
14. Jenkin, M. E.; Saunders, S. M.; Wagner, V.; Pilling, M. J., Protocol for the development of the master chemical mechanism, mcm v3 (part b): Tropospheric degradation of aromatic volatile organic compounds. *Atmos. Chem. Phys.* **2003**, 3, (1), 181.
15. Bloss, C.; Wagner, V.; Jenkin, M. E.; Volkamer, R.; Bloss, W. J.; Lee, J. D.; Heard, D. E.; Wirtz, K.; Martin-Reviejo, M.; Rea, G.; Wenger, J. C.; Pilling, M. J., Development of a detailed chemical mechanism (mcmv3.1) for the atmospheric oxidation of aromatic hydrocarbons. *Atmos. Chem. Phys.* **2005**, 5, (3), 641.